COBEM 2023 27TH INTERNATIONAL CONGRESS OF MECHANICAL ENGENEERING

ABCM Brazilian Society of Mechanical Sciences and Engineering
27th ABCM International Congress of Mechanical Engineering
December 04-08, 2023, Florianópolis-SC, Brazil

COB-2023-1758
INFLUENCE OF CARREAU-YASUDA MODEL PARAMETERS ON NAJAFI-GOLESTANIAN MICROSWIMMER SWIMMING IN GENERALIZED NEWTONIAN FLUID

Gustavo Alves Lima
Instituto Federal do Espírito Santo (IFES) – Campus São Mateus, São Mateus-ES, Brazil, CEP: 29932-540.
2001gustavoalves@gmail.com

Roberto Frederico Ausas
José Alberto Cuminato
Gustavo Carlos Buscaglia
Instituto de Ciências Matemáticas e de Computação, Universidade de São Paulo, São Carlos-SP, Brazil. CEP 13566-590.
rfausas@icmc.usp.br
jacumina@icmc.usp.br
gustavo.buscaglia@icmc.usp.br

Stevens Paz
Departamento de Matemáticas, Universidad del Valle, Calle 13 No. 100-00, Cali, Colombia
stevens.paz@correounivalle.edu.co

Abstract. *Microswimmers can be defined as self-propelled organisms capable of independent locomotion. The study of microswimmers has contributed significantly to advancements in various fields, including biology and biomedicine. Given the diverse range of fluids in which microswimmers may operate during practical applications, there is a growing need for computational analyses of their swimming performance in complex scenarios that closely mimic real-world fluid behavior. This includes non-Newtonian fluids, which can be characterized using the Carreau-Yasuda model. This study aims to investigate the impact of viscous parameters within the Carreau-Yasuda model on the swimming behavior of Najafi-Golestanian microswimmers, applying the optimal swimming policy. Numerical experiments were conducted, demonstrating the method's convergence with mesh refinement and time step reduction. The analysis of the Carreau-Yasuda model's coefficient n and characteristic time λ showed that, for n<1, the average swimming velocity increases (for n≥0.2, it is up to 17.8% greater than the swimming velocity in a Newtonian fluid), while it decreases for n < 1.*

Keywords: *Microswimmers, Non-Newtonian fluid, Najafi-Golestanian swimmer.*

1. INTRODUCTION

Microswimmer analysis has been a prominent subject of study in recent decades, greatly contributing to comprehension of the locomotion of microscopic biological components, such as cell movement, and its applications in biomedicine, including drug transport (Nganglia et al., 2020). One fundamental microswimmer model was proposed by Najafi and Golestanian (2004). In this model, three rigid spheres (B_1, B_2, and B_3) are arranged in a linear configuration and interconnected by two filaments with negligible thickness and lengths L_1 and L_2, as illustrated in Figure 1. The contraction and expansion of these filaments changes the distance between adjacent spheres, allowing the microswimmer to move in a straight line (Najafi and Golestanian, 2004; Paz et al., 2022).

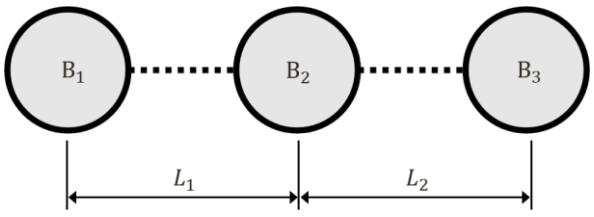

Figure 1. Swimmer of three spheres by Najafi and Golestanian (2004).

In practical applications, microswimmers can be subjected to diverse flow conditions, necessitating an evaluation of how fluid dynamic parameters impact their performance (Coclite et al., 2020). The study of swimming in non-Newtonian

fluids is significant as many essential fluids exhibit such behavior, including blood and mucus (Nganglia et al., 2020; Calejo, 2013). The Carreau-Yasuda model is a widely used approach for approximating viscosity in several applications documented in the literature, including the analysis of squirmer microswimmer locomotion (Nganglia et al., 2020), pipe flow analysis (Andrade et al., 2007), flow over a pore space (Khan et al., 2019), and the development of blood-like fluids (Calejo, 2013).

According to the Carreau-Yasuda model, fluid viscosity can be approximated by

$$\mu = \mu_\infty + (\mu_0 - \mu_\infty) \cdot [1 + (\lambda \cdot |\dot{\gamma}|)^2]^{\frac{n-1}{2}},$$

where μ_0 represents the apparent viscosity of the fluid at zero shear rate, μ_∞ is a reference viscosity, λ is a characteristic temporal measure, n is an exponent characterizing the non-Newtonian behavior of the fluid, and γ is the strain rate tensor.

Thus, this work aimed to evaluate the behavior of the three-ball microswimmer in a non-Newtonian fluid, analyzing the influence of the n and λ parameters on its velocity in a swimming cycle. In section 2, the basic equations that model the problem are showed. Section 3 provides an analysis of the simulator's convergence. The results of the swimming assessment are detailed and discussed in Section 4, and the study's conclusions are summarized in Section 5.

2. GOVERNING EQUATIONS

Assuming no external forces act upon the microswimmer, the hydrodynamic problem is characterized as follows. It involves an analysis of the microswimmer's hydrodynamic behavior, taking into account the velocity field (u) and pressure field (p) within the context of an incompressible fluid. Additionally, it is assumed that the Reynolds number tends toward zero, signifying that inertial forces are negligible compared to viscous effects.

Let Ω be the domain containing the spheres B_i (where $B\_i = \{x \in R^3 | \, |x - C\_i| \leq R\}$, with R representing the radius of the sphere centered at C_i, $i = 1,2,3$) and the fluid $\Omega_f = \Omega - B_1 - B_2 - B_3$. According to (Paz et al., 2022), the equations governing the motion of the microswimmer are given by

$$\nabla \cdot \boldsymbol{\sigma} = \mathbf{0} \text{ in } \Omega_f, \tag{2}$$

$$\nabla \cdot \boldsymbol{u} = 0 \text{ in } \Omega_f, \tag{3}$$

$$\int_{\partial B} \boldsymbol{\sigma} \cdot \hat{\boldsymbol{n}} \, dS = 0, \tag{4}$$

$$\boldsymbol{u} = \left(\frac{dX}{dt} - \frac{2}{3}\frac{dL_1}{dt} - \frac{1}{3}\frac{dL_2}{dt}\right) \hat{\boldsymbol{e}} \text{ on } \partial B_1, \tag{5}$$

$$\boldsymbol{u} = \left(\frac{dX}{dt} + \frac{1}{3}\frac{dL_1}{dt} - \frac{1}{3}\frac{dL_2}{dt}\right) \hat{\boldsymbol{e}} \text{ on } \partial B_2, \tag{6}$$

$$\boldsymbol{u} = \left(\frac{dX}{dt} + \frac{1}{3}\frac{dL_1}{dt} + \frac{2}{3}\frac{dL_2}{dt}\right) \text{ on } \partial B_3, \tag{7}$$

where

$$\boldsymbol{\sigma} = -p\boldsymbol{I} + \mu(\nabla \boldsymbol{u} + \nabla \boldsymbol{u}^T) \tag{8}$$

is the Cauchy stress of the fluid, and $X = (C_1 + C_2 + C_3)/3$ is the center of mass of the microswimmer. Equations (2, 3) correspond to the Stokes equations, with Eq. (3) representing the incompressibility condition. Eq. (4) enforces the force-free condition with $\hat{\boldsymbol{n}}$ being the outward unit normal to Ω_f. Equations (5, 6, 7) impose the non-slip condition on the surface of each sphere, where $\hat{\boldsymbol{e}}$ is the unit vector indicating the direction of motion. Boundary conditions on Ω_f simulate an infinite domain. In this study, this system of equations is numerically solved using the Finite Element Method within the FEniCS platform, with a Python interface. The solution is obtained by applying Newton's Method to solve the associated nonlinear system.

In this study, spheres with a radius of $R = 1\mu$m were employed, where the maximum and minimum distances between their centers were 3.1μm and 2.1μm, respectively. The Ω_f domain corresponds to the volume extending from $B = B_1 \cup B_2 \cup B_3$ to a 300μm x 150μm rectangle, as shown in Figure 2.

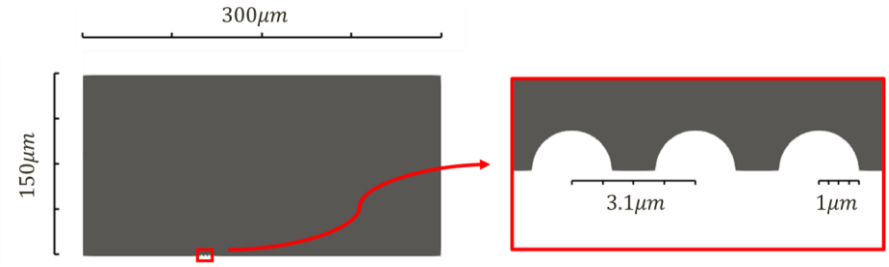

Figure 2. Computational domain of the problem in the initial state.

The swimming policy determines the sequence of contractions and expansions of the microswimmer's left and right ligaments. Figure 3 illustrates the swimming policy that ensures the maximum displacement per cycle in a Newtonian fluid, referred to as the optimal policy, as described in (Paz et al., 2022).

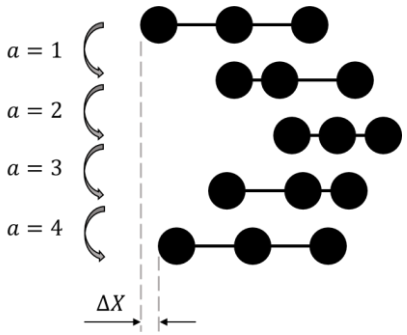

Figure 3. Representation of the swimming policy adopted in this work. In the figure, a is the action performed and ΔX is the net displacement per cycle.

In this study, we adopt $\mu_0 = 2$ and $\mu_\infty = 1$ in the Carreau-Yasuda model. If $n > 1$, the viscosity increases (shear-thickening fluid), and if $n < 1$, the viscosity decreases (shear-thinning fluid). The viscosity behavior is depicted in Figure 4, according to the variation of the product $\lambda \cdot |\dot{\gamma}|$. It's worth noting that for values of n close to 1 or λ close to 0, the fluid behaves similarly to a Newtonian fluid with a viscosity of $\mu_0 = 2$.

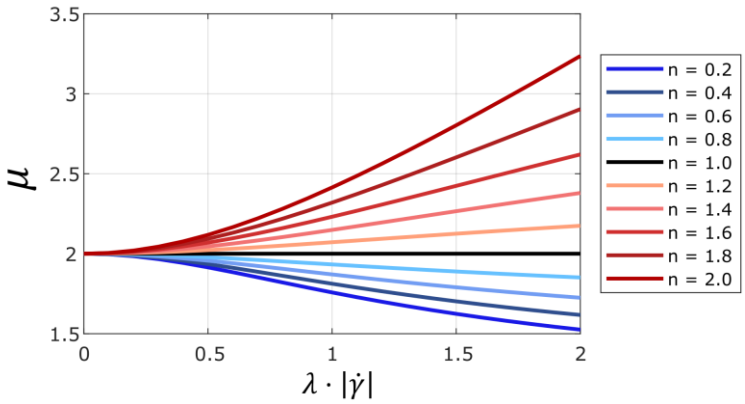

Figure 4. Variation of viscosity according to product $\lambda \cdot |\dot{\gamma}|$ for some values of n.

3. CONVERGENCE ANALYSIS

For the mesh analysis, two parameters were varied: the R1 parameter, which influences mesh refinement near the sphere, and the R2 parameter, which affects mesh refinement farther from the sphere. Smaller values for R1 and R2 result in a finer mesh. Additionally, variations were made to the time interval for temporal progression (Δt) and the n and λ parameters of the Carreau-Yasuda model, as detailed in Table 1. In total, 2800 simulations were conducted, and for each simulation, data on the number of iterations required by Newton's method for solving the nonlinear system, the position of a swimmer's reference point over time, and the number of mesh nodes were collected.

Table 1. Values adopted for the analysis variables.

Parameter	Values used
R1	1/4, 1/8, 1/16, 1/32 e 1/64
R2	1/2, 1/4, 1/8 e 1/16
Δt	0.5, 0.2, 0.1 e 0.05
λ	0.8, 1, 1.2, 10 e 20.
n	0.2, 0.5, 0.8, 1, 1.2, 1.5 e 2

Initially, the convergence of the Newton solver was assessed with respect to the viscosity parameters, determining which sets of parameters (pairs of n and λ) yielded the highest number of iterations. The results are presented in Table 2.

Table 2. Average and maximum number of iterations used to solve the nonlinear system by Newton's method.

		Average number of iterations					Maximum number of iterations				
	λ	0,8	1	1,2	10	20	0,8	1	1,2	10	20
	0,2	3,28	3,29	3,30	3,28	3,24	5	5	5	5	5
	0,5	3,18	3,20	3,21	3,24	3,24	5	5	5	5	5
	0,8	2,94	2,97	2,98	3,10	3,12	5	5	5	5	5
n	1	1,00	1,00	1,00	1,00	1,00	1	1	1	1	1
	1,2	2,99	3,02	3,05	3,26	3,29	5	5	5	6	6
	1,5	3,41	3,43	3,47	3,89	4,01	7	7	7	8	8
	2	4,02	4,13	-	-	-	23	18	-	-	-

It's noteworthy that difficulties arose in solving the problem for cases with $n = 2$. In contrast, the method demonstrated successful convergence in all other scenarios. As a result, subsequent analyses focus solely on the remaining 2400 simulations.

The evaluation of the relative error in the simulations, based on mesh parameters and the time step, was conducted regarding a reference solution. The adopted reference solution was the most critical situation of the analyzed variables (parameters R1 = 1/64, R2 = 1/16 and Δt = 0.05 s) with the same fluid properties. Relative error was determined by examining the total displacement of a reference point on the swimmer. For each swimming cycle, n_r pairs of time and position were identified in the reference solution. An equivalent number of pairs was then located in the simulation for comparison, utilizing linear interpolation. This led to the quantification of simulation error according to

$$Error = \sqrt{\frac{\sum_{i=1}^{n_r}(x_i^r - x_i^p)^2}{\sum_{i=1}^{n_r}(x_i^r)^2}}, \tag{9}$$

in which x_i^r and x_i^p represent the position in the reference solution and the solution being compared at time instant i. The results are graphically presented in Figure 5, while Table 3 provides a overview of the minimum and maximum errors observed across all simulations sharing the same set of parameters (R1, R2, Δt).

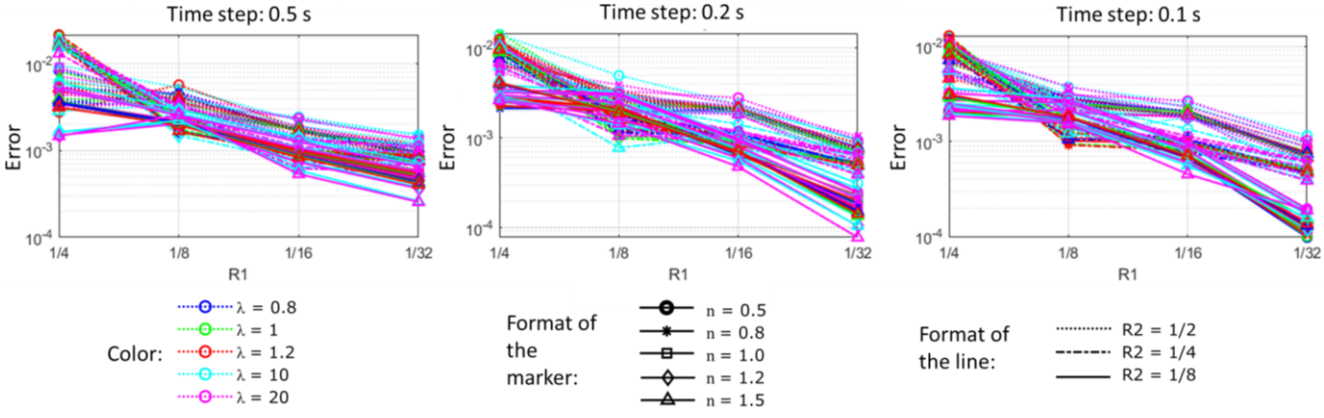

Figure 5. Error obtained in the convergence analysis simulations.

Table 3. Minimum and maximum errors obtained in all simulations performed with the same trio (R1, R2, Δt).

Δt	R1	Minimal erros				Maximum errors			
		R2				R2			
		1/2	1/4	1/8	1/16	1/2	1/4	1/8	1/16
0.5	1/4	2.77E-03	1.31E-02	1.47E-03	2.05E-03	9.66E-03	2.16E-02	6.14E-03	5.31E-03
	1/8	2.71E-03	1.49E-03	1.97E-03	1.02E-03	5.71E-03	3.23E-03	2.96E-03	2.65E-03
	1/16	1.37E-03	6.27E-04	5.37E-04	8.08E-04	2.44E-03	1.44E-03	1.39E-03	1.34E-03
	1/32	5.46E-04	5.47E-04	2.55E-04	3.30E-04	1.54E-03	1.20E-03	7.44E-04	7.81E-04
	1/64	5.04E-04	3.14E-04	2.50E-04	2.51E-04	1.16E-03	7.21E-04	6.73E-04	6.44E-04
0.2	1/4	5.50E-03	4.10E-03	2.13E-03	1.04E-03	1.46E-02	1.25E-02	4.12E-03	4.94E-03
	1/8	1.89E-03	7.75E-04	1.36E-03	6.86E-04	4.94E-03	2.41E-03	3.26E-03	2.49E-03
	1/16	1.78E-03	7.64E-04	4.77E-04	7.18E-04	2.78E-03	1.41E-03	1.01E-03	1.06E-03
	1/32	4.96E-04	3.90E-04	7.78E-05	2.17E-04	1.04E-03	6.87E-04	3.10E-04	3.72E-04
	1/64	3.48E-04	1.40E-04	8.79E-05	4.30E-05	6.16E-04	2.63E-04	2.01E-04	9.61E-05
0.1	1/4	3.40E-03	5.77E-03	1.86E-03	1.22E-03	1.00E-02	1.29E-02	3.63E-03	3.91E-03
	1/8	1.12E-03	9.21E-04	1.56E-03	6.73E-04	3.76E-03	2.57E-03	2.82E-03	2.66E-03
	1/16	1.78E-03	7.66E-04	4.55E-04	6.47E-04	2.67E-03	1.35E-03	1.01E-03	1.03E-03
	1/32	4.56E-04	3.89E-04	9.88E-05	2.02E-04	1.15E-03	6.50E-04	1.97E-04	3.67E-04
	1/64	3.46E-04	1.42E-04	4.13E-05	1.62E-05	7.75E-04	2.29E-04	1.21E-04	8.57E-05

It's important to observe that the relative error exhibited a higher magnitude in less dense meshes, while its sensitivity to the time step remained relatively modest. Table 4 presents the maximum error obtained for each mesh parameter, irrespective of the selected time step.

Table 4. Highest error obtained in the simulations for each pair of mesh refinement parameters.

		R2			
		1/2	1/4	1/8	1/16
R1	1/4	1.00E-02	1.29E-02	3.63E-03	3.91E-03
	1/8	3.76E-03	2.57E-03	2.82E-03	2.66E-03
	1/16	2.67E-03	1.35E-03	1.01E-03	1.03E-03
	1/32	1.15E-03	6.50E-04	1.97E-04	3.67E-04
	1/64	7.75E-04	2.29E-04	1.21E-04	8.57E-05

Table 5 shows the average number of mesh nodes for each pair of parameters R1 and R2. This data aids in the identification of the optimal pair of R1 and R2 parameters. In consideration of an error tolerance of 10^{-3}, it is worth noting that employing R1 = 1/32 and R2 = 1/4 yields the lowest average number of mesh nodes. This outcome implies a more efficient computational performance, suggesting that this parameter combination is a favorable choice.

Table 5. Mesh average number of nodes according to the variation of parameters R1 and R2.

		R2			
		1/2	1/4	1/8	1/16
R1	1/4	264	543	1410	2433
	1/8	443	715	1215	2409
	1/16	981	1544	2034	3630
	1/32	2541	3391	4932	6678
	1/64	7545	9242	12165	16935

The numerical analysis revealed that for values of n less than 1, the Newton's method efficiently solved the nonlinear system within as few as 5 iterations, with an average of approximately 3 iterations. However, for values of n greater than 1, the simulator required a higher number of iterations to achieve convergence. Notably, when n equaled 2, non-convergent results were encountered, rendering it an unsuitable choice for the implemented algorithm. It is worth noting that by adopting mesh parameters R1 = 1/32 and R2 = 1/4, favorable results were achieved at a lower computational cost. A sample mesh employed in the analysis is depicted in Figure 6. The time step demonstrated minimal impact, with the longest interval (0.5 s) proving sufficient. These parameters were subsequently employed in the ensuing analysis.

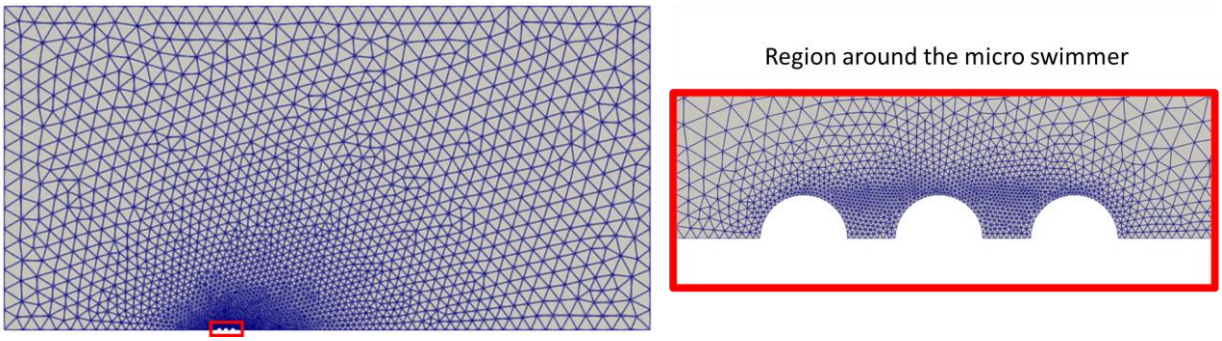

Figure 6. Mesh with R1 = 1/32 and R2 = 1/4 at the initial instant.

4. ANALYSIS OF THE MICROSWIMMER'S MOVEMENT

To assess swimming performance, variations were introduced in the λ and n parameters as outlined in Table 6.

Table 6. Values adopted for the analysis parameters.

Parameter	Values used
λ	From 0 to 20, increasing by 2
n	From 0.2 to 1.6, increasing by 0.2

In each simulation, the body's displacement was recorded, enabling the calculation of the average velocity. The average velocity of the microswimmer for various pairs of parameters λ and n (V) was compared with the body's velocity in a Newtonian fluid (V_n). Figure 7 shows the ratio between the average velocity of a swimming cycle in the non-Newtonian fluid and the velocity in the Newtonian fluid (V/V_n) as a function of the viscous parameters.

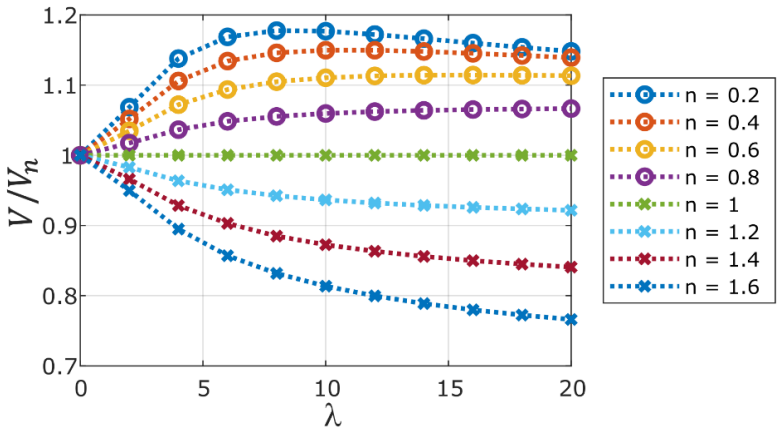

Figure 7. Variation of the V/V_N ratio as a function of parameters λ and n.

Note that in shear-thickening fluids ($n > 1$) the swimmer has its velocity reduced with the increase of λ, and the swimming velocity is always lower than in a Newtonian fluid. In shear-thinning fluids ($n < 1$), the average velocity is greater than the velocity in the Newtonian fluid. The graphical analysis suggests that, setting a value of λ between 6 and 10, the speed presents a value of λ that confers maximum speed in shear-thinning fluids, becoming more evident at a lower value of n. Figure 8 highlights the velocity variation for $n = 1.6$ (representing shear-thickening fluid) and $n = 0.2$ (representing shear-thinning fluid).

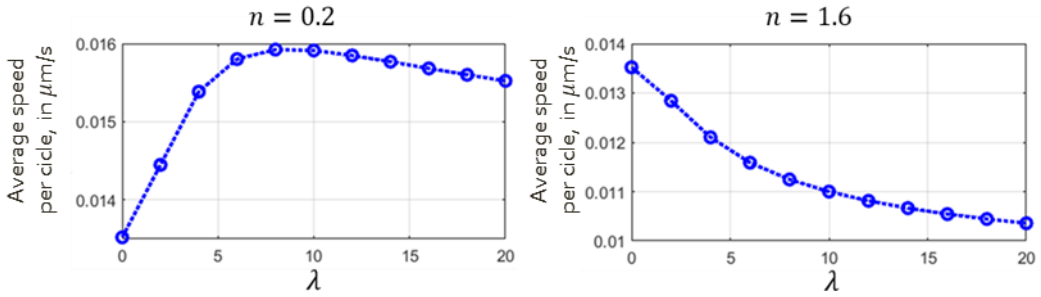

Figure 8. Average swimmer speed as a function of λ for $n = 1.6$ and $n = 0.2$.

It is also observed in Figure 7 that, for the same parameter λ, the velocity decreases with the increase of n, regardless of whether the fluid is shear-thickening or shear-thinning, as illustrated in Figure 9.

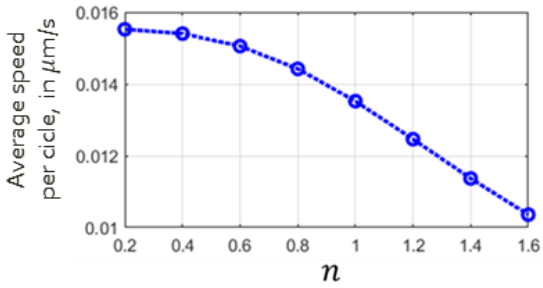

Figure 9. Variation of average swimming speed as a function of n for $\lambda = 20$.

It's important to highlight that the overall displacement of the body is relatively minor when compared to the individual displacements in each motion of the swimmer. Figure 10 provides a visualization of the body's displacement for scenarios involving $n = 0.2$ and $n = 1.6$, while considering λ values of 0, 8, and 20.

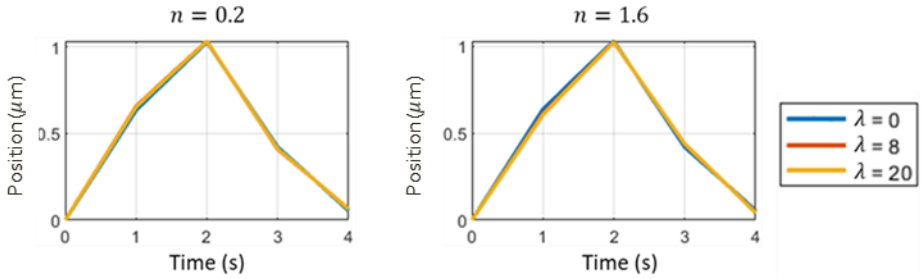

Figure 10. Position of the micro swimmer as a function of time, for $n = 0.2$ and 1.6.

The displacements following each action of the microswimmer, as presented in Figure 10, are summarized in Table 7, including the net displacement per swim cycle. It is worth highlighting that, for $\lambda = 8$ and $n = 0.2$, the swimmer covers a distance of 0.0637 μm, 17.8% more than a cycle in a Newtonian fluid, which registers at 0.0541 μm. This stands as the highest increase found in the simulations performed.

Table 7. Displacement of the micro swimmer after each action of the swimming cycle, in μm.

n		0.2		0.2 or 1.6	1.6	
λ		8	20	0[(1)]	8	20
Swim cycle action	$a = 1$	0.6563	0.6525	0.6351	0.6115	0.6042
	$a = 2$	0.5201	0.5194	0.5168	0.5135	0.5126
	$a = 3$	-0.1274	-0.1242	-0.1103	-0.0904	-0.0847
	$a = 4$	-0.4810	-0.4817	-0.4842	-0.4875	-0.4884
Net displacement per cycle		0.0637	0.0621	0.0541	0.0450	0.0414

(1) Newtonian case.

Figures 11 and 12 depict the evolution of fluid behavior over time and with varying λ parameters in the context of shear thickening. It's evident that as λ increases, regions characterized by higher viscosity emerge between the spheres, corresponding to areas with more significant velocity gradients.

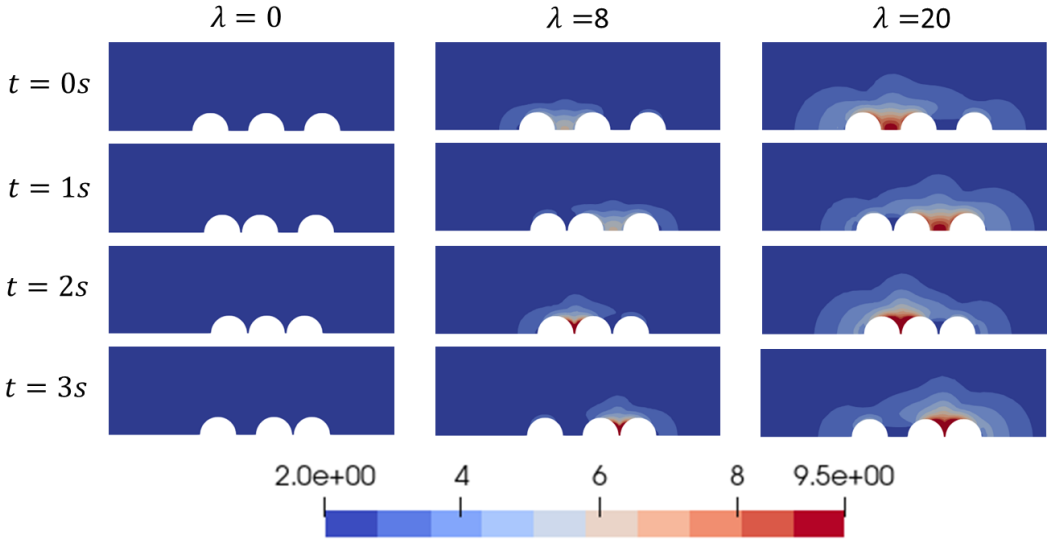

Figure 11. Fluid viscosity for $n = 1.6$ according the movement action and λ parameter, in Pa s.

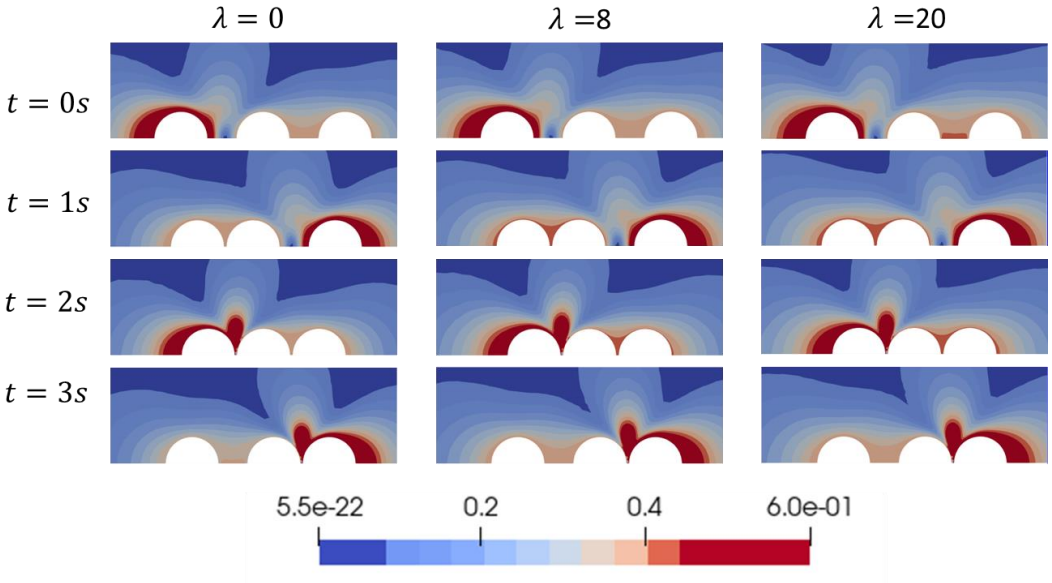

Figure 12. Fluid velocity for $n = 1.6$ according the movement action and λ parameter, in μm/s.

Figures 13 and 14 illustrate the transformation of fluid behavior over time and with varying λ parameters in the context of shear thinning. It's noteworthy that as λ increases, regions characterized by reduced viscosity become increasingly prominent.

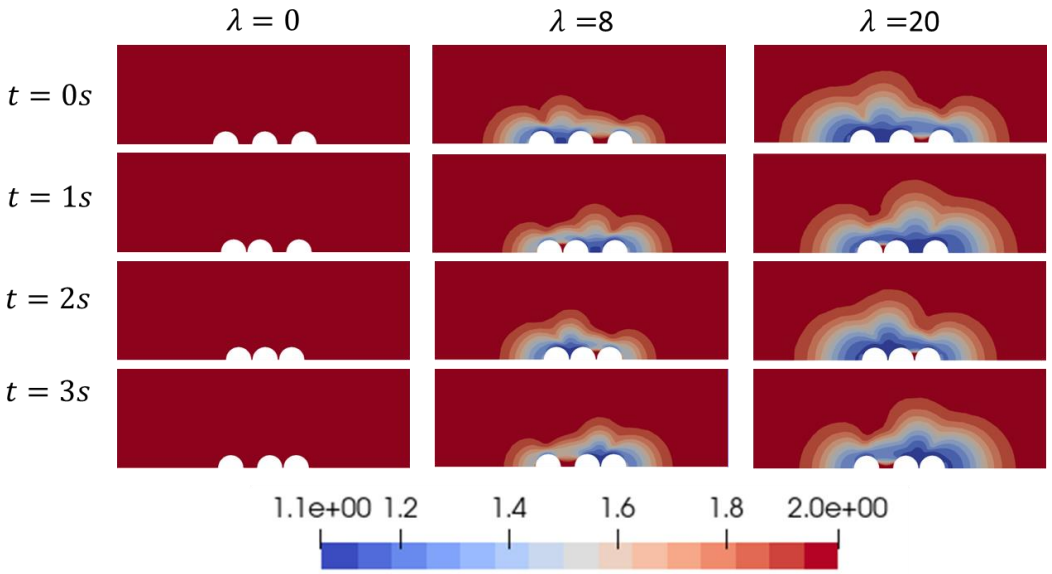

Figure 13. Fluid viscosity for $n = 0.2$ according the movement action and λ parameter, in Pa s.

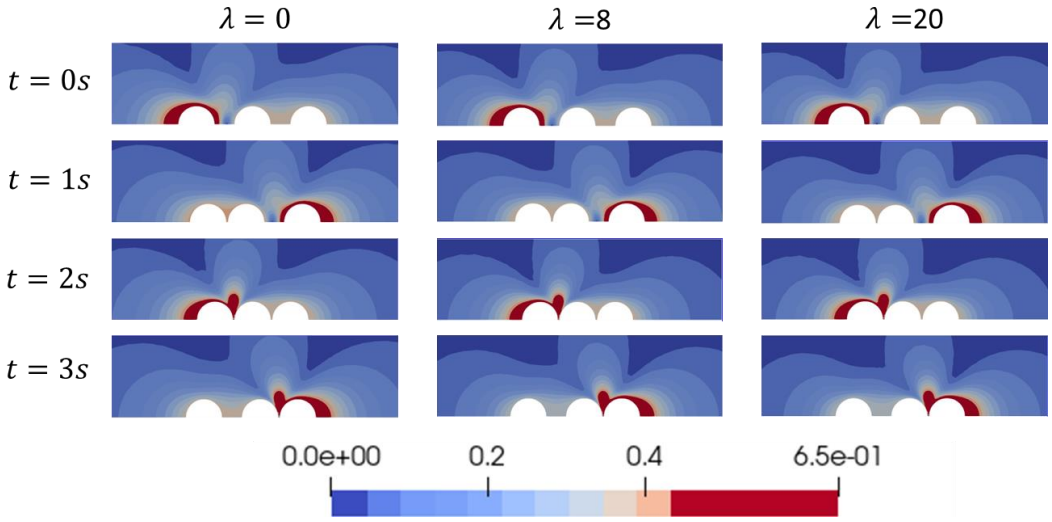

Figure 14. Fluid velocity for $n = 0.2$ according the movement action and λ parameter, in μm/s.

5. CONCLUSION

This study presents a computational analysis of the swimming behavior of a three-sphere microswimmer in a fluid characterized by the Carreau-Yasuda model. The analysis involved varying the parameters λ from 0 to 20 and n from 0.2 to 1.6, with a comparison of swimming performance against the behavior in a Newtonian fluid. Additionally, a numerical assessment of method convergence was included.

The findings indicated that shear-thinning fluids enhanced the microswimmer's speed, with the degree of enhancement inversely proportional to the value of n. Furthermore, for a fixed n value, there existed an optimal λ value that maximized velocity. The highest observed increase reached 17.8% above the swimming speed in a Newtonian fluid.

Additionally, in shear-thickening fluids, the microswimmer's swimming velocity in a cycle was lower compared to that in a Newtonian fluid. The degree of reduction intensified with increasing deviation of viscosity from Newtonian behavior, characterized by larger values of λ and n.

6. ACKNOWLEDGEMENTS

The authors thankfully acknowledge financial support from the São Paulo Research Foundation (FAPESP) under grants 2022/11659-2. We thank for CEPID-CeMEAI and the São Paulo University in the association with the Aristides Pacheco Leão Program. This work yet was partially supported by the FAPES, FAPEMIG, CNPq and CAPES.

7. REFERENCES

Andrade, L. C. F., Petronílio, J. A., Maneschy, C. E. D. A., and Cruz, D. O. D. A., 2007. The carreau-yasuda fluids: a skin friction equation for turbulent flow in pipes and kolmogorov dissipative scales. *Journal of the Brazilian Society of Mechanical Sciences and Engineering*, 29, 162-167.

Calejo, J. A. C. *Development of Biphasic Fluids Analogous to Blood: Rheological Study, Flow in Microchannels and Numerical Simulations (in Portuguese).* Master's thesis. Escola Superior de Tecnologia e Gestão, Instituto Politécnico de Bragança, Portugal, 2013.

Coclite, A; Coclite, G. M.; de Tommasi, D., 2020. Capsules Rheology in Carreau–Yasuda Fluids. *Nanomaterials*, v. 10, n. 11, p. 2190.

Khan, M. I. et al., 2020. Theoretical and numerical investigation of Carreau–Yasuda fluid flow subject to Soret and Dufour effects. *Computer methods and programs in biomedicine*, v. 186, p. 105145.

Najafi, A.; Golestanian, R., 2004. Simple swimmer at low Reynolds number: Three linked spheres. *Physical Review E*, v. 69, n. 6, p. 062901.

Nganguia, H.; zheng, K.; Chen, Y.; Pak, O. S.; Zhu, L., 2020. A note on a swirling squirmer in a shear-thining fluid. *Phyisics on Fluids*.

Paz, S.; Ausas, R. F.; Carbajal, J. P.; Buscaglia, G. C., 2022. Chemoreception and chemotaxis of a three-sphere swimmer. Communications in Nonlinear Science and Numerical Simulation. *Communications in Nonlinear Science and Numerical Simulations*.

Paz, S.; Buscaglia, G. C., 2020. Simulating squirmers with volumetric solvers. *Journal of the Brazilian Society of Mechanical Sciences and Engineering.*

8. RESPONSIBILITY NOTICE

The authors are the only responsible for the printed material included in this paper.